The 2-chloroquinolin-6-ol (**9**), which was prepared from quinolin-2,6-diol by selective chlorination, was used for the synthesis of the 6-hydroxy substituted 2-arylquinoline derivatives **10** (THK-5272) and **11** via Suzuki coupling reaction (Scheme 1C). THK-5273 (**12**) was obtained by a nucleophilic substitution reaction with methylamine from **11**.

To estimate the blood–brain barrier permeability of hydroxyquinoline derivatives, logP values were measured by an HPLC method and found to range from 0.5 to 1.3 (Table 1). These data indicated that the hydroxyquinoline derivatives have sufficient lipophilicity to penetrate the blood–brain barrier.[27]

To evaluate the tau fibril binding characteristics of the synthesized hydroxyquinoline derivatives, we carried out fluorescence analyses (Figure 2). Fluorescence of the dye thioflavin-T or thioflavin-S increases when they bind to amyloid fibrils including fibrils from recombinant tau constructs.[30,32] Similar to these dyes, BF-158 derivatives show enhanced fluorescence intensities upon binding to a cross β-sheet structure. The results from the fluorescence binding assays using recombinant K18Δ280K-tau fibrils indicated that the fluorescence enhancement of THK-951 and THK-5272 was observed in the presence of tau fibrils (Figure 2A, G). In contrast, the pyridine-containing derivatives, THK-953 and THK-5273, showed little change in fluorescence intensity or, interestingly, slightly weakening in the present of tau fibrils (Figure 2D, J). The elaborate verification of the cause of this fluorescence change was not examined in the present study, but the possibility of a quenching effect caused by the binding conformation of the compounds is presumed.

Subsequently, fluorescent staining using AD hippocampal sections was performed to examine the in vitro binding affinity of the tested compounds for tau pathology in AD tissues. THK-951 clearly stained NFTs and neuropil threads in the hippocampal section of an AD brain under a blue filter (Figure 2B, C). THK-5272 also stained NFTs but with a lower contrast image compared with THK-951 (Figure 2E, F). The neuropathological staining with BF-170, which is a dehydroxylated derivative of THK-5272, showed high affinity for NFTs rather than SPs[26]; thus, a contribution from the substituted position of the hydroxyl group to the affinity for NFTs was indicated. THK-953 (Figure 2H, I) and THK-5273 (Figure 2K, L) are highly fluorescent compounds, but very weak images of tau pathology were observed in this study. These results correlated with the results from the fluorescence binding assay using recombinant tau fibrils and indicated that the quinoline-pyridine derivatives bind very little to regions of tau pathology or have low binding affinity easily removable by a brief wash.

For further comparison of the binding affinity of hydroxyquinoline derivatives for recombinant tau fibrils, we determined their K_i values in competition with [^{18}F]THK-523, a tau imaging probe for PET. The K_i values of THK-951, THK-953, THK-5272, and THK-5273 were 20.7, 110.4, 36.1, and 30.4, respectively (Table 1). THK-951 had the highest affinity for tau fibrils from the hydroxyquinoline derivatives tested. In contrast with the image obtained for its fluorescent staining, THK-5273 showed comparable affinity with THK-5272. The weak staining of THK-5273 was probably caused by its high sensitivity to the washing technique used or the absence of a fluorescent hyperchromic effect compared with THK-5272.

Table 1. Lipophilicity (logP) and binding affinity (K_i values) of hydroxyquinoline derivatives to recombinant tau fibrils

Compound name	X	R_1	R_2	logP*	K_i (nM)
THK-951	C	$NHCH_3$	7-OH	1.28	20.7
THK-953	N	$NHCH_3$	7-OH	0.56	110.4
THK-5272	C	NH_2	6-OH	0.61	36.1
THK-5273	N	$NHCH_3$	6-OH	0.90	30.4

*logP values were determined by HPLC method.

In this study, the quinoline derivatives with higher lipophilicities had lower K_i values. For Aβ ligands, it is considered that the lipophilicity of the ligand correlates with the degree of nonspecific binding but is not correlated with its binding affinity for Aβ fibrils.[6,33] It is possible that the lipophilicity of a compound has a considerable effect on its binding affinity for the cross β-sheet structures of tau; however, more structure–activity related studies are needed to understand this further.

Following the results of the fluorescence assays and competitive binding assay, we selected THK-951 for additional studies using a radiolabeled ligand, with consideration of the availability of THK-951 for a tau PET probe. Radiolabeling of THK-951 was performed using an *N*-Boc and *O*-TBDMS protected precursor (**15**) and [^{11}C]MeOTf (Scheme 2). [^{11}C]THK-951 was obtained in yields of 39% on average with radiochemical purity greater than 99% after HPLC purification. The average specific activity of [^{11}C]THK-951 was 83.2 GBq/μmol.

The poor brain kinetics of a PET tracer can harm the quantitative performance of a PET study, so high blood–brain barrier permeability and rapid clearance from the brain are essential for brain imaging agents. To evaluate the brain kinetics of [^{11}C]THK-951, we carried out an ex vivo biodistribution study using normal mice (Table 2). [^{11}C]THK-951 showed rapid brain uptake (3.23 ± 0.27% ID/g at 2 min) and smooth washout from the normal brain (0.11 ± 0.01% ID/g at 60 min), resulting to a high 2-min-to-60 min ratio (29.4) of brain uptake of [^{11}C]THK-951. This uptake ratio in a normal mouse brain is superior to that of [^{18}F]THK-523 (1.86), [^{18}F]THK-5105 (9.20), or [^{18}F]THK-5117 (23.1),[28] indicating that our structural optimization worked as intended. Compared with these ^{18}F-labeled tracers, the binding affinity of [^{11}C]THK-951 for tau aggregates is slightly lower, but the superiority in brain kinetics could make up for its weakness in binding affinity. It is known that the concentrations of tau aggregates are lower than those of Aβ in an AD brain[22]; therefore, a higher elimination efficiency of the free radiotracer from the brain would be more important for tau probes than for Aβ probes. The fast clearance of [^{11}C]THK-951 from a normal mouse brain is likely caused by its low lipophilicity. The uptake in the kidney was highest at 2 min postinjection (19.8 % ID/g) followed by a fast clearance. The uptake in the liver showed a slow clearance after 10 min postinjection, while the radioactivity in the small intestine increased with time, indicating the biliary excretion of radioactive agents.

Finally, as an assessment of the binding affinity of [^{11}C]THK-951 for the regions of tau pathology, ARG analysis using AD hippocampal sections was performed. The ARG image showed high accumulation of [^{11}C]THK-951 in the CA1 region of the AD hippocampus (Figure 3A). Distribution of the tracer signal of [^{11}C]THK-951 correlated well with that of [^{18}F]THK-523 (Figure 3B) and tau immunostaining (Figure 3C). On the other hand, the distribution of the tracer signal was different from the immunostained Aβ pathology, which showed spotty distribution in that region (Figure 3D).

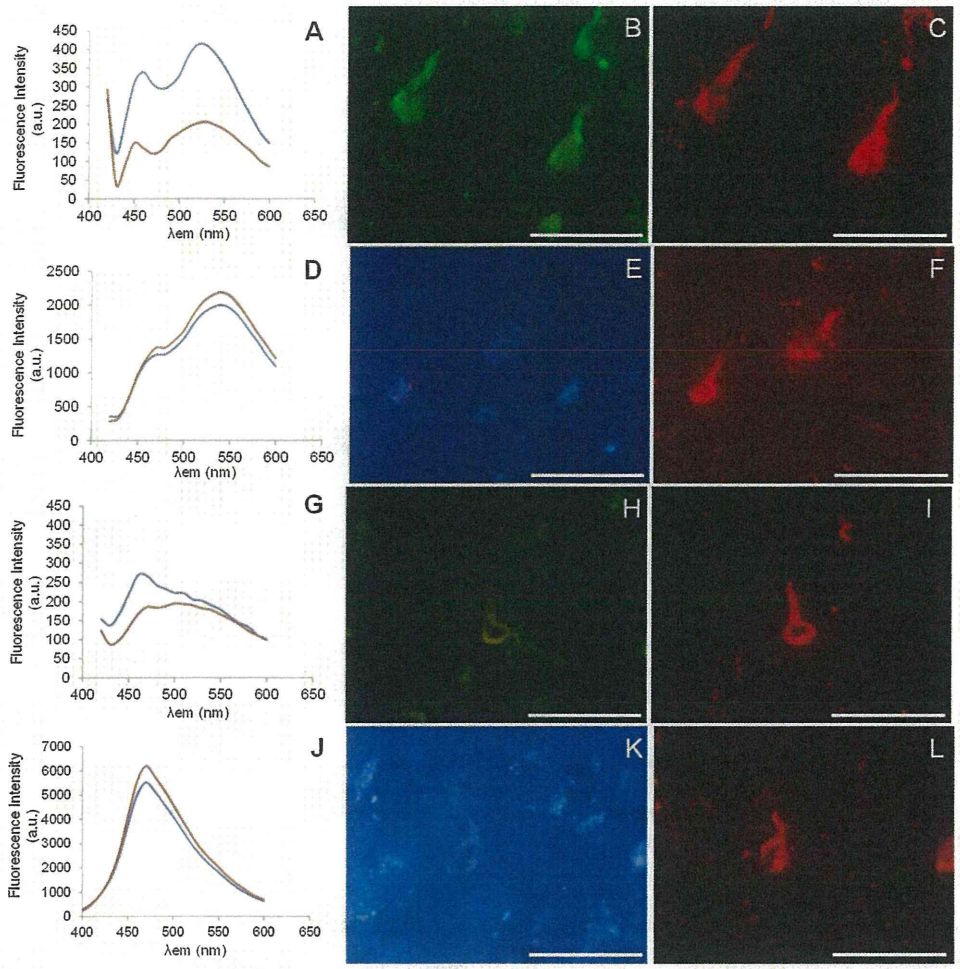

Figure 2. Fluorescence spectral analyses and neuropathological staining of THK-951 (A–C), THK-953 (D–F), THK-5272 (G–I), and THK-5273 (J–L). (A, D, G, and J) Fluorescence spectra of THK-951 (A, λ_{ex} = 390 nm), THK-953 (D, λ_{ex} = 390 nm), THK-5272 (G, λ_{ex} = 390 nm), and THK-5273 (J, λ_{ex} = 360 nm) in the presence or absence of K18Δ280K-tau fibrils (K18Δ280K-tau: blue lines; control (ligands only): red lines). (B, C, E, F, H, I, K, and L) Double staining with hydroxyquinoline derivatives and anti-pTau antibody (AT8). (B, E, H, and K) Fluorescent staining of hippocampal sections from cases of Alzheimer's disease (THK-951: B; THK-953: E; THK-5272: H; THK-5273: K). (C, F, I, and L) Immunostaining by AT8. Scale bars: 50 μm. This figure is available in color online at wileyonlinelibrary.com/journal/jlcr

Table 2. Biodistribution of [^{11}C]THK-951 in ICR mice

Tissue	2 min	10 min	30 min	60 min	90 min
Blood	2.65 (0.46)	1.20 (0.48)	0.20 (0.04)	0.12 (0.01)	0.11 (0.02)
Brain	3.23 (0.27)	0.81 (0.13)	0.15 (0.05)	0.11 (0.01)	0.06 (0.01)
Liver	10.14 (2.66)	10.00 (1.79)	1.99 (0.45)	1.10 (0.23)	0.85 (0.27)
Kidney	19.79 (6.77)	4.10 (0.34)	0.96 (0.43)	0.49 (0.11)	0.35 (0.09)
Small intestine	4.72 (1.44)	12.22 (3.10)	24.91 (3.17)	29.33 (2.23)	24.64 (1.83)

Data are expressed as mean of % ID/g (Standard Deviation) (n = 4).

These results indicated that [^{11}C]THK-951 was promising in its ability to bind regions of tau pathology in the AD brain.

In vivo tau imaging will allow the accurate measurement of the distribution of tau pathology in the AD brain. The combined assessments of tau burden and other biomarkers of AD (e.g., Aβ burden, brain metabolism, and clinical findings) are needed to understand the accurate pathogenic mechanism or time course of AD.[4] One of the advantages of developing ^{11}C-labeled tau probes is that tau probes labeled with this short-half-life radionuclide will facilitate two PET studies in the same day by using other PET probes such as [^{18}F]FDG or Aβ PET after the tau imaging.

To develop probes with ideal brain kinetics, we introduced a hydroxyl group at the 6 or 7 position of quinoline. Lipophilicity has considerable influences on not only tracer kinetics but also binding affinity; therefore, lipophilicity needs to be optimized for tau tracers. In this study, the properties of [^{11}C]THK-951 (logP = 1.28) were balanced between achieving high binding affinity for tau fibrils and blood–brain permeability with a fast clearance from mouse brain. We plan to evaluate other derivatives having different hydroxylated positions or alkyl amino groups to obtain additional structure–activity relationship information.

A competitive binding assay using a radiolabeled ligand may ensure the examination of tau binding ligands, which do not seem to have binding affinity for tau pathology in a fluorescence

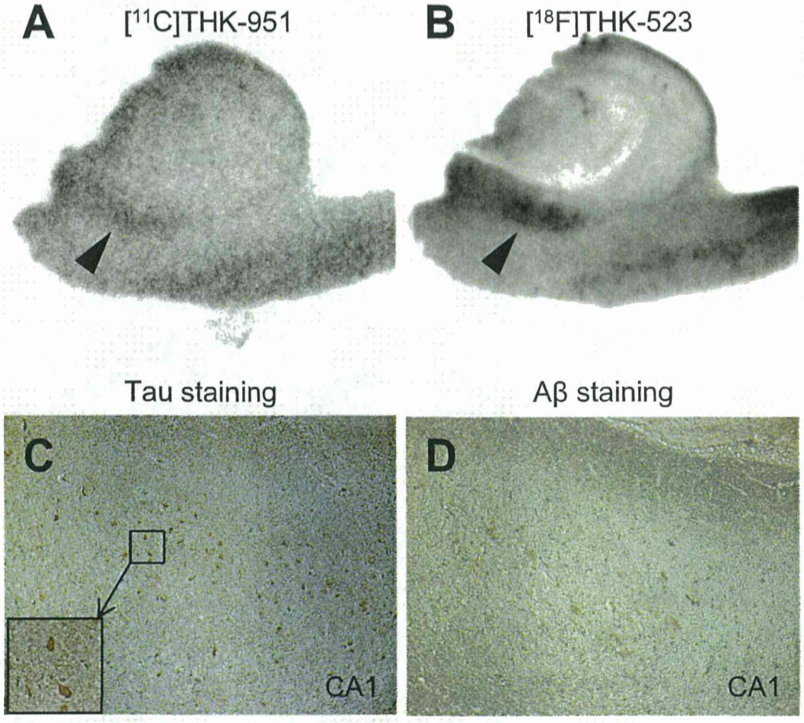

Figure 3. Characterization of in vitro binding of [^{11}C]THK-951 to tau pathology by autoradiography and immunohistochemistry. [^{11}C]THK-951 showed high accumulation in the hippocampal CA1 region (A, filled arrowhead). Similarly, [^{18}F]THK-523, a well-characterized tau probe, also highly accumulated in the CA1 region (B, filled arrowhead). Immunostaining of adjacent sections demonstrated that numerous tau immunopositive neurofibrillary tangles were observed in CA1 region (C). By contrast, Aβ staining showed weak immunoreactivity in CA1 region (D).

binding assay using AD brain sections. On the other hand, some researchers indicated that the PHFs constructed from tau fragments do not fully conform to the structure of PHFs from an AD brain.[22,32] Thus, these in vitro binding assay results should be considered carefully, and comparison with the results from future clinical studies would facilitate our selection of an evaluation method.

Conclusion

We synthesized four hydroxyquinoline derivatives and performed biological evaluations to estimate their potential as tau imaging probes. From these results, we selected THK-951 for additional studies and successfully radiosynthesized [^{11}C]THK-951. [^{11}C]THK-951 showed ideal brain kinetics in normal mice, and its binding affinity for regions of tau pathology was confirmed by an in vitro ARG assay using AD hippocampal sections. Further evaluation of THK-951 and structurally optimized derivatives will facilitate our understanding about AD tau pathology in the living body.

Acknowledgements

This study was supported by the Industrial Technology Research Grant Program of the NEDO (09E51025a) in Japan, the Health and Labour Sciences Research Grants from the Ministry of Health, Labour, and Welfare of Japan, Grant-in-Aid for Scientific Research (B) (23390297), and the 'Japan Advanced Molecular Imaging Program (J-AMP)' of the Ministry of Education, Culture, Sports, Science, and Technology of Japan.

Conflict of Interest

This study was supported by the research fund from GE Healthcare.

References

[1] K. Ogomori, T. Kitamoto, J. Tateishi, Y. Sato, M. Suetsugu, M. Abe, *Am. J. Pathol.* **1989**, *134*, 243–51.
[2] H. Braak, E. Braak, *Acta Neuropathol.* **1991**, *82*, 239–59.
[3] P. M. Thompson, K. M. Hayashi, G. de Zubicaray, A. L. Janke, S. E. Rose, J. Semple, D. Herman, M. S. Hong, S. S. Dittmer, D. M. Doddrell, A. W. Toga, *J. Neurosci.* **2003**, *23*, 994–1005.
[4] C. R. Jack, D. S. Knopman, W. J. Jagust, R. C. Petersen, M. W. Weiner, P. S. Aisen, L. M. Shaw, P. Vemuri, H. J. Wiste, S. D. Weigand, T. G. Lesnick, V. S. Pankratz, M. C. Donohue, J. Q. Trojanowski, *Lancet Neurol.* **2013**, *12*, 207–16.
[5] E. D. Agdeppa, V. Kepe, J. Liu, S. Flores-torres, N. Satyamurthy, A. Petric, G. M. Cole, G. W. Small, S. Huang, J. R. Barrio, *J. Neurosci.* **2001**, *21*, 1–5.
[6] C. A. Mathis, Y. Wang, D. P. Holt, G. Huang, M. L. Debnath, W. E. Klunk, *J. Med. Chem.* **2003**, *46*, 2740–2754.
[7] S. R. Choi, G. Golding, Z. Zhuang, W. Zhang, N. Lim, F. Hefti, T. E. Benedum, M. R. Kilbourn, D. Skovronsky, H. F. Kung, *J. Nucl. Med.* **2009**, *50*, 1887–94.
[8] Y. Kudo, N. Okamura, S. Furumoto, M. Tashiro, K. Furukawa, M. Maruyama, M. Itoh, R. Iwata, K. Yanai, H. Arai, *J. Nucl. Med.* **2007**, *48*, 553–561.
[9] M.-P. Kung, C. Hou, Z.-P. Zhuang, B. Zhang, D. Skovronsky, J. Q. Trojanowski, V. M.-Y. Lee, H. F. Kung, *Brain res.* **2002**, *956*, 202–10.
[10] M. M. Svedberg, O. Rahman, H. Hall, *Nucl. Med. Biol.* **2012**, *39*, 484–501.
[11] V. L. Villemagne, K. E. Pike, D. Darby, P. Maruff, G. Savage, S. Ng, U. Ackermann, T. F. Cowie, J. Currie, S. G. Chan, G. Jones, H. Tochon-Danguy, G. O'Keefe, C. L. Masters, C. C. Rowe, *Neuropsychologia* **2008**, *46*, 1688–97.

[12] C. M. Clark, J. A. Schneider, B. J. Bedell, T. G. Beach, W. B. Bilker, M. A. Mintun, M. J. Pontecorvo, F. Hefti, A. P. Carpenter, M. L. Flitter, M. J. Krautkramer, H. F. Kung, R. E. Coleman, C. H. Sadowsky, E. M. Reiman, S. P. Zehntner, D. M. Skovronsky, *JAMA* **2011**, *305*, 275–284.
[13] K. Herholz, K. Ebmeier, *Lancet Neurol.* **2011**, *10*, 667–70.
[14] V. L. Villemagne, K. E. Pike, G. Chételat, K. A. Ellis, R. S. Mulligan, P. Bourgeat, U. Ackermann, G. Jones, C. Szoeke, O. Salvado, R. Martins, G. O'Keefe, C. A. Mathis, W. E. Klunk, D. Ames, C. L. Masters, C. C. Rowe, *Ann. Neurol.* **2011**, *69*, 181–92.
[15] V. M. Lee, B. J. Balin, L. Otvos, J. Q. Trojanowski, *Science* **1991**, *251*, 675–8.
[16] R. Medeiros, D. Baglietto-Vargas, F. M. LaFerla, *CNS Neurosci. Ther.* **2011**, *17*, 514–24.
[17] P. V. Arriagada, J. H. Growdon, E. T. Hedley-Whyte, B. T. Hyman, *Neurology* **1992**, *42*, 631–631.
[18] D. W. Dickson, *Neurobiol. Aging* **1997**, *18*, S21–S26.
[19] P. T. Nelson, G. A. Jicha, F. A. Schmitt, H. Liu, D. G. Davis, M. S. Mendiondo, E. L. Abner, W. R. Markesbery, *J. Neuropathol. Exp. Neurol.* **2007**, *66*, 1136–46.
[20] P. T. Nelson, I. Alafuzoff, E. H. Bigio, C. Bouras, H. Braak, N. J. Cairns, R. J. Castellani, B. J. Crain, P. Davies, K. Del Tredici, C. Duyckaerts, M. P. Frosch, V. Haroutunian, P. R. Hof, C. M. Hulette, B. T. Hyman, T. Iwatsubo, K. A. Jellinger, G. A. Jicha et al., *J. Neuropathol. Exp. Neurol.* **2012**, *71*, 362–81.
[21] L. E. Rojo, J. Alzate-Morales, I. N. Saavedra, P. Davies, R. B. Maccioni, *J. Alzheimers Dis.* **2010**, *19*, 573–89.
[22] V. Villemagne, S. Furumoto, M. T. Fodero-Tavoletti, R. Harada, R. S. Mulligan, Y. Kudo, C. L. Masters, K. Yanai, C. C. Rowe, N. Okamura, *Future Neurol.* **2012**, *7*, 409–421.
[23] D. T. Chien, S. Bahri, A. K. Szardenings, J. C. Walsh, F. Mu, M.-Y. Su, W. R. Shankle, A. Elizarov, H. C. Kolb, *J. Alzheimer's Dis.* **2013**, *34*, 457–68.
[24] C.-F. Xia, J. Arteaga, G. Chen, U. Gangadharmath, L. F. Gomez, D. Kasi, C. Lam, Q. Liang, C. Liu, V. P. Mocharla, F. Mu, A. Sinha, H. Su, A. K. Szardenings, J. C. Walsh, E. Wang, C. Yu, W. Zhang, T. Zhao et al., *Alzheimer's Dement.* **2013**, *in press*, doi: 10.1016/j.jalz.2012.11.008.
[25] W. Zhang, J. Arteaga, D. K. Cashion, G. Chen, U. Gangadharmath, L. F. Gomez, D. Kasi, C. Lam, Q. Liang, C. Liu, V. P. Mocharla, F. Mu, A. Sinha, A. K. Szardenings, E. Wang, J. C. Walsh, C. Xia, C. Yu, T. Zhao et al., *J. Alzheimer's Dis.* **2012**, *31*, 601–12.
[26] N. Okamura, T. Suemoto, S. Furumoto, M. Suzuki, H. Shimadzu, H. Akatsu, T. Yamamoto, H. Fujiwara, M. Nemoto, M. Maruyama, H. Arai, K. Yanai, T. Sawada, Y. Kudo, *J. Neurosci.* **2005**, *25*, 10857–62.
[27] M. T. Fodero-Tavoletti, N. Okamura, S. Furumoto, R. S. Mulligan, A. R. Connor, C. A. McLean, D. Cao, A. Rigopoulos, G. A. Cartwright, G. O'Keefe, S. Gong, P. A. Adlard, K. J. Barnham, C. C. Rowe, C. L. Masters, Y. Kudo, R. Cappai, K. Yanai, V. L. Villemagne, *Brain* **2011**, *134*, 1089–100.
[28] N. Okamura, S. Furumoto, R. Harada, T. Tago, T. Yoshikawa, M. Fodero-Tavoletti, R. S. Mulligan, V. L. Villemagne, H. Akatsu, T. Yamamoto, H. Arai, R. Iwata, K. Yanai, Y. Kudo, *J. Nucl. Med.* **2013**, *54*, 1420–7.
[29] OECD GUIDELINE FOR THE TESTING OF CHEMICALS, Partition coefficient (n-octanol/water), high performance liquid chromatography (HPLC) method, doi: 10.1787/9789264069824-en.
[30] S. Barghorn, E. Mandelkow, *Biochemistry* **2002**, *41*, 14885–96.
[31] N. Okamura, T. Suemoto, H. Shimadzu, M. Suzuki, T. Shiomitsu, H. Akatsu, T. Yamamoto, M. Staufenbiel, K. Yanai, H. Arai, H. Sasaki, Y. Kudo, T. Sawada, *J. Neurosci.* **2004**, *24*, 2535–41.
[32] M. Biancalana, S. Koide, *Biochim. Biophys. Acta 2010*, **1804**, 1405–12.
[33] A. Forsberg, A. Juréus, Z. Cselényi, M. Eriksdotter, Y. Freund-Levi, F. Jeppsson, B.-M. Swahn, J. Sandell, P. Julin, M. Schou, J. Andersson, P. Johnström, K. Varnäs, C. Halldin, L. Farde, S. Svensson, *Eur. J. Nucl. Med. Mol. Imaging* **2013**, *40*, 580–93.

Supporting information

Additional supporting information may be found in the online version of this article at the publisher's web site.

Eur J Nucl Med Mol Imaging (2014) 41:816–826
DOI 10.1007/s00259-013-2681-7

ORIGINAL ARTICLE

In vivo evaluation of a novel tau imaging tracer for Alzheimer's disease

Victor L. Villemagne · Shozo Furumoto · Michelle T. Fodero-Tavoletti · Rachel S. Mulligan · John Hodges · Ryuichi Harada · Paul Yates · Olivier Piguet · Svetlana Pejoska · Vincent Doré · Kazuhiko Yanai · Colin L. Masters · Yukitsuka Kudo · Christopher C. Rowe · Nobuyuki Okamura

Received: 14 October 2013 / Accepted: 20 December 2013 / Published online: 11 February 2014

Abstract
Purpose Diagnosis of tauopathies such as Alzheimer's disease (AD) still relies on post-mortem examination of the human brain. A non-invasive method of determining brain tau burden in vivo would allow a better understanding of the pathophysiology of tauopathies. The purpose of the study was to evaluate ^{18}F-THK523 as a potential tau imaging tracer.

Methods Ten healthy elderly controls, three semantic dementia (SD) and ten AD patients underwent neuropsychological examination, MRI as well as ^{18}F-THK523 and ^{11}C-Pittsburgh compound B (PIB) positron emission tomography (PET) scans. Composite memory and non-memory scores, global and hippocampal brain volume, and partial volume-corrected tissue ratios for ^{18}F-THK523 and ^{11}C-PIB were estimated for all participants. Correlational analyses were performed between global and regional ^{18}F-THK523, ^{11}C-PIB, cognition and brain volumetrics.
Results ^{18}F-THK523 presented with fast reversible kinetics. Significantly higher ^{18}F-THK523 retention was observed in the temporal, parietal, orbitofrontal and hippocampi of AD patients when compared to healthy controls and SD patients. White matter retention was significantly higher than grey matter retention in all participants. The pattern of cortical ^{18}F-THK523 retention did not correlate with Aβ distribution as assessed by ^{11}C-PIB and followed the known distribution of tau in the AD brain, being higher in temporal and parietal areas than in the frontal region. Unlike ^{11}C-PIB, hippocampal ^{18}F-THK523 retention was correlated with several cognitive parameters and with hippocampal atrophy.
Conclusion ^{18}F-THK523 does not bind to Aβ in vivo, while following the known distribution of paired helical filaments (PHF)-tau in the brain. Significantly higher cortical ^{18}F-THK523 retention in AD patients as well as the association of hippocampal ^{18}F-THK523 retention with cognitive parameters and hippocampal volume suggests ^{18}F-THK523 selectively binds to tau in AD patients. Unfortunately, the very high ^{18}F-THK523 retention in white matter precludes simple visual inspection of the images, preventing its use in research or clinical settings.

Keywords Alzheimer's disease · Tau imaging · Aβ Imaging · Neurodegeneration · Brain

Electronic supplementary material The online version of this article (doi:10.1007/s00259-013-2681-7) contains supplementary material, which is available to authorized users.

V. L. Villemagne · M. T. Fodero-Tavoletti · R. S. Mulligan · P. Yates · S. Pejoska · V. Doré · C. C. Rowe
Centre for PET, Austin Health, Melbourne, Australia

V. L. Villemagne · M. T. Fodero-Tavoletti · C. L. Masters
The Mental Health Research Institute, Melbourne, Australia

S. Furumoto · R. Harada · K. Yanai · N. Okamura
Department of Pharmacology, Tohoku University School of Medicine, Sendai, Japan

J. Hodges · O. Piguet
Neuroscience Research Australia, Sydney, Australia

J. Hodges · O. Piguet
The University of New South Wales, Sydney, Australia

V. Doré
Preventative Health Flagship, CSIRO ICT, Brisbane, Australia

Y. Kudo
Innovation of New Biomedical Engineering Center, Tohoku University, Sendai, Japan

V. L. Villemagne (✉)
Department of Nuclear Medicine and Centre for PET, Austin Health, 145 Studley Rd, Heidelberg, VIC 3084, Australia
e-mail: villemagne@petnm.unimelb.edu.au

Introduction

Most neurodegenerative conditions are characterized by the aggregation of a misfolded protein such as Aβ and tau in Alzheimer's disease (AD), transactive response (TAR) DNA binding protein 43 kDa (TDP-43) in some forms of frontotemporal lobar degeneration (FTLD) such as semantic dementia (SD) or α-synuclein in Parkinson's disease. Tauopathies are neurodegenerative diseases characterized by the pathological accumulation of aggregated tau. AD is the most common tauopathy and the leading cause of dementia [1], but tau deposits are also found in other variants of FTLD, such as progressive non-fluent aphasia (PNFA) or in some cases of behavioural frontotemporal dementia (bFTD) [2]. Other tauopathies include Down's syndrome, Guam parkinsonism-dementia complex, frontotemporal dementia with parkinsonism linked to chromosome 17, corticobasal degeneration, progressive supranuclear palsy and chronic traumatic encephalopathy [3–5]. Definitive diagnosis of these neurodegenerative conditions can only be established after death. While these tauopathies share tau immunoreactivity in post-mortem brain examination, these tau aggregates can be composed of different tau isoforms displaying very distinct histopathological and ultrastructural differences [3, 6, 7]. In AD, these tau deposits can be recognized histologically as neurofibrillary tangles (NFTs) and neuropil threads as well as dystrophic neurites in senile plaques, whilst ultrastructurally they aggregate in paired helical filaments (PHF) [3, 4, 8]. While the underlying mechanisms leading to tau hyperphosphorylation, misfolding and aggregation remain unclear, tau aggregation and deposition follows a stereotypical and spatiotemporal pathway both at the intraneuronal level [8, 9] as well as in its topographical and neuroanatomical distribution in the brain [4, 10, 11].

The notion that tau dysregulation is a key mediator of neurodegeneration [12, 13] has stimulated the development of therapeutics for the treatment of AD and non-AD tauopathies [14–16]. Given these treatments are currently being developed, a non-invasive method of determining the tau burden in the brain would allow a better understanding of the pathophysiology of AD, FTLD and other tau-related neurodegenerative conditions. It will also lead to improvements in differential diagnostic accuracy and accelerate drug discovery by facilitating patient selection and monitor efficacy in novel anti-tau therapeutic trials. It would assist in the early and differential diagnosis of AD and non-AD tauopathies, while helping ascertain the relationship between the spatiotemporal distribution of tau aggregates in the brain to cognition and brain volumetrics. Development of tau imaging probes poses several more challenges than those associated with Aβ imaging, and these are mainly related to the idiosyncrasies of tau aggregation and deposition. In contrast to Aβ, most tau aggregates are intracellular, there are six tau isoforms and the different combinations of these isoforms manifest as different clinical phenotypes. Tau aggregates undergo a wide spectrum of post-translation modifications that, in addition to the combination of different isoforms, lead to diverse ultrastructural conformations and typical pathological lesions. Furthermore, tau aggregates coexist with other misfolded proteins sharing the same β-sheet secondary structure, as is in the case of AD where tau and Aβ are both co-localized in grey matter areas, where the concentrations of Aβ are, depending on the brain region, ~5–20 times higher than those of tau (for an in depth review see Villemagne et al. [17]).

In recent years, the main focus has been the development of selective ligands that allow early detection of Aβ deposition [18]. Among these tracers, ^{18}F-FDDNP was reported to non-selectively bind to both Aβ deposits and NFTs [19]. Phenylquinoline derivatives binding with high affinity and selectivity for tau aggregates have been developed as candidates for tau imaging agents at Tohoku University in Sendai, Japan [20]. Among them, ^{18}F-THK523 (THK523) was the first reported selective tau imaging tracer that can non-invasively detect tau deposits in a transgenic mouse brain [21]. This report was recently followed by several other potential tau tracer candidates [22–27].

After a careful in vitro evaluation, the initial in vivo characterization of a novel positron emission tomography (PET) neuroligand candidate requires to fulfill certain conditions such as safety at low tracer doses, possess high affinity and selectivity for the target, ability to cross the blood–brain barrier, display low non-specific binding with adequate regional distribution and its relation to parameters known to be associated with the intended target, suitable brain kinetics, lack of problematic radiolabelled metabolites [28] before it is applied to research or clinical use (Supplementary Fig. 1).

Therefore, the main objective of the present study was to characterize the in vivo suitability of THK523 for tau imaging in humans. The in vivo assessment comprised: (a) comparing the global and regional THK523 binding in healthy controls (HC), AD and SD patients, (b) assessing the relationship between THK523 retention and cognition, (c) assessing the relationship between THK523 retention and brain volumetrics and (d) comparing the regional brain distribution of THK523 with that of ^{11}C-Pittsburgh compound B (PIB) in the same participants.

Materials and methods

Participants

Written informed consent was obtained from all participants. Approval for the study was obtained from the Austin Health Human Research Ethics Committee. Elderly HC were recruited by advertisement in the community and dementia patients

were recruited from tertiary Memory Disorders Clinics or from physicians who sub-specialize in dementia care. All participants were classified on the basis of their clinical and neuropsychological performance by consensus of a neurologist and a neuropsychologist. Individuals classified as HC performed within normal limits on cognitive tests. AD patients met NINCDS-ADRDA criteria for probable AD [29], while three FTLD patients were classified as SD [30, 31]. None of the AD or FTLD patients had a family history of dementia.

Safety evaluation

Clinical, haematological and biochemical data on the safety of THK523 were collected for all participants. Heart rate, blood pressure, temperature and respiratory rate were measured immediately prior to injection and at 2, 15, 60 and 180 min post-injection. Immediately prior to THK523 injection, blood was drawn for routine haematology and biochemistry tests. An ECG was performed prior to injection of THK523 and at the completion of the scan, when they were also questioned for adverse events. All subjects were contacted by telephone 24 h later and questioned for adverse events. Between 5 and 8 days post-injection, subjects returned to be questioned for adverse events and for a physical examination, including a set of observations and repeat haematology and biochemistry testing.

Neuropsychological evaluation

In addition to the Mini-Mental State Examination (MMSE), Clinical Dementia Rating (CDR) and Clinical Dementia Rating Sum of Boxes (CDR SOB), the primary cognitive performance measures were composite episodic memory and non-memory scores generated as previously described [32]. Briefly, a composite episodic memory score was calculated by taking the average of the z scores (generated using 65 HC with both low PIB and normal MRI as the reference) for Rey Complex Figure Test (RCFT, 30 min) Long Delay and California Verbal Learning Test - Second Edition (CVLT-II) Long Delay and Logical Memory II. A composite non-memory score was calculated by taking the average of the z scores for the Boston Naming Test, letter fluency, category fluency, digit span forwards and backwards, digit symbol-coding and RCFT copy.

Image acquisition

Magnetic resonance imaging

Participants received an MRI on a 3 T Siemens TRIO MRI system (Siemens Healthcare, Erlangen, Germany) using the Alzheimer's Disease Neuroimaging Initiative (ADNI) 3D magnetization prepared rapid acquisition gradient echo (MPRAGE) sequence with 1×1 mm in-plane resolution and 1.2-mm slice thickness, repetition time (TR)/echo time (TE)/T1-weighted=2,300/2.98/900, flip angle 9° and field of view 240×256 and 160 slices. T2 -weighted fast spin-echo (FSE) and fluid-attenuated inversion recovery (FLAIR) sequences were also obtained. The interval between the THK523 and MRI studies was 1.6±3.3 months.

Positron emission tomography

Productions of ^{11}C-PIB and ^{18}F-THK523 were performed in the Centre for PET, Austin Hospital. ^{11}C-PIB was synthesized using the one-step ^{11}C-methyl triflate approach as previously described [18]. The decay-corrected average radiochemical yield for ^{11}C-PIB was 30 % with a radiochemical purity of >98 % and a specific activity of 30±7. 5 GBq/μmol. ^{18}F-THK523 was synthesized by nucleophilic substitution of the tosylate precursor [BF-241, 2-3 mg in 700 μl dimethyl sulphoxide (DMSO)]. The decay-corrected average radiochemical yield of the production of ^{18}F-THK523 was 22.5±5 %, with a radiochemical purity of>95 % and a specific activity of 225.6±134.8 GBq/μmol (6.2±3.3 Ci/μmol).

A 30-min acquisition (6×5-min frames) on an Allegro™ PET camera started 40 min after injection of 300 MBq ^{11}C-PIB intravenously. A 90-min list-mode emission acquisition was performed in 3D mode after injection of 200 MBq ^{18}F-THK523. List-mode raw data were sorted offline into 6×30-s, 7×1-min, 4×2.5-min, 2×5-min and 6×10-min frames. The sorted sinograms were reconstructed using a 3D row action maximum likelihood algorithm (RAMLA). The interval between the THK523 and PIB PET studies was 0.3±3.8 months.

Tracer metabolism

Compound stability was assessed by incubating the tracer for 5, 30, 60, 90, 180 and 240 min with human S9 liver fractions.

Image analysis

Magnetic resonance imaging

Hippocampal and cortical grey matter volumes were obtained using a commercial fully automated volumetric measurement program (NeuroQuant®) applied to the 3D MPRAGE MRI images. The primary MRI performance measures were the grey cortical matter and hippocampal volumes normalized for total intracranial volume.

Positron emission tomography

PET images were processed using a semi-automatic region of interest (ROI) method as previously described [32]. Briefly,

THK523 and PIB PET images were co-registered to each individual's MRI using SPM8 (Wellcome Trust Centre for Neuroimaging, London, UK), and the same ROI template was applied. Given the reversible nature of THK523 kinetics, distribution volume ratios (DVR) were determined through graphical analysis of the dynamic data. Standardized uptake value ratios (SUVR) for PIB and THK523 as well as THK523 DVR were generated using the cerebellar cortex as reference region [18, 33]. Global tau and Aβ burden were expressed as the average SUVR for the following cortical ROIs: frontal (consisting of dorsolateral prefrontal, ventrolateral prefrontal and orbitofrontal regions), superior parietal, lateral temporal, lateral occipital and anterior and posterior cingulate for THK523 and PIB, respectively. As in previous studies, a PIB SUVR threshold of 1.5 was used to categorize high (PIB+) and low (PIB−) Aβ burden [32].

Partial volume correction (PVC), accounting for *both* grey matter atrophy and white matter spillover, was performed applying a three-compartment approach using PMOD 3.1 (PMOD Technologies Ltd., Zurich, Switzerland). DVR for THK523 were determined through graphical analysis of the last 45 min of the 90-min acquisition [33]. In order to avoid arterial blood sampling, a simplified approach was applied using the cerebellar cortex as reference region [18, 33]. Global DVR was calculated with the same regions used for the global SUVR. The primary outcome measure used for all THK523 and PIB assessments was the PVC SUVR.

Statistical evaluation

Normality of distribution was tested using the Shapiro-Wilk test and visual inspection of variable histograms. Statistical evaluations to establish differences between clinical groups means were performed using a Tukey-Kramer HSD test and by a Dunnett's test to compare each group with controls. Pearson's product-moment correlation analyses were conducted between imaging and clinical variables. Categorical differences were evaluated using Fisher's exact test. Effect size was measured with Cohen's *d*. All analyses were adjusted for age and corrected for multiple comparisons using false discovery rates. Data are presented as mean±standard deviation unless otherwise stated.

Results

Participants

Demographic characteristics of the participants are shown in Table 1. As expected, there were significant differences between the AD and SD patients and HC in cognitive performance and brain volumetrics. The AD group also presented with significantly higher PIB retention. While there were no significant differences between groups in age and gender, the AD group was less educated. While seven of the HC and the three SD patients showed low PIB retention, three of the HC presented with high PIB retention (Table 1).

No adverse events related to the study drug were observed or reported by participants or carers following the THK523 scan. There were no significant changes in clinical or biochemical parameters.

Tracer metabolism

THK523 was minimally metabolized, with 91, 81 and 65 % of unchanged parent compound remaining at 30, 90 and 180 min, respectively. No lipophilic radiometabolites were observed.

Brain kinetics

Brain THK523 radioactivity peaked between 3 and 6 min post-injection and the binding appeared to be reversible with rapid clearance from the brain (Fig. 1a, b). THK523 cleared fastest from cerebellar cortex and the clearance rate was the same for all groups (Fig. 1a, b). Clearance was slower from cortical areas in AD (Fig. 1b) than in HC (Fig. 1a) and SD patients. The ratio of cortical to cerebellar binding became constant in all participants by 50 min after injection (Fig. 1c).

Visual inspection

Visual inspection of the summed 60–90-min SUVR images revealed significantly higher THK523 retention in white matter than in grey matter regions, being significantly higher in AD patients than in HC or SD (Fig. 1d).

Assessment of tau burden

Regional analysis showed that there were no group differences in cerebellar cortex THK523 SUV, and there was no correlation between cerebellar cortex THK523 SUV with age in the whole cohort or with dementia severity in the AD group as assessed by MMSE (r=0.25, p=0.50), CDR (r=0.13, p=0.72) or CDR SOB (r=0.03, p=0.94).

While 60–90-min THK523 SUVR was estimated for all participants, four participants (two HC and two AD) were not able to complete the initial THK523 dynamic scan preventing calculation of DVR. In the remaining 16 subjects, significantly higher THK523 DVR were found in AD subjects in all cortical regions. The global THK523 DVR was 1.02±0.15 in AD vs 0.86±0.11 in HC (p=0.04, Cohen's effect size d=1.2). No significant differences were observed between HC and SD patients. Similar findings were observed with THK523

Table 1 Demographics

	HC (n=10)	SD (n=3)	AD (n=10)
Age	77.4±10.0	65.6±8.1	75.6±9.5
Gender (M/F)	3/7	1/2	4/6
MMSE	29.3±1.1	21.7±1.2*	16.7±6.6*
CDR	0.0	0.8±0.3*	1.3±0.6*
CDR SOB	0.1±0.2	2.5±1.1*	7.3±4.5*
Years of education	14.7±2.7	12.5±4.9	11.5±3.6*
Episodic memory scores	−0.4±0.6	−1.9±0.9*	−3.8±0.5*
Non-memory scores	−0.1±0.4	−1.4±1.2*	−3.4±1.6*
Hippocampal volume (cm^3)	5.1±0.6	4.3±0.3	4.1±1.0*
Aβ burden (PIB SUVR)	1.5±0.6 [PIB−=1.2±0.1 (n=7)] [PIB+=2.2±0.6 (n=3)]	1.1±0.1	2.9±0.5*

MMSE Mini-Mental State Examination, *CDR* Clinical Dementia Rating, *CDR SOB* Clinical Dementia Rating Sum of Boxes, *PIB* Pittsburgh compound B, *SUVR* standardized uptake value ratio, *PIB−* low PIB retention, *PIB+* high PIB retention

*Significantly different from HC (p<0.05)

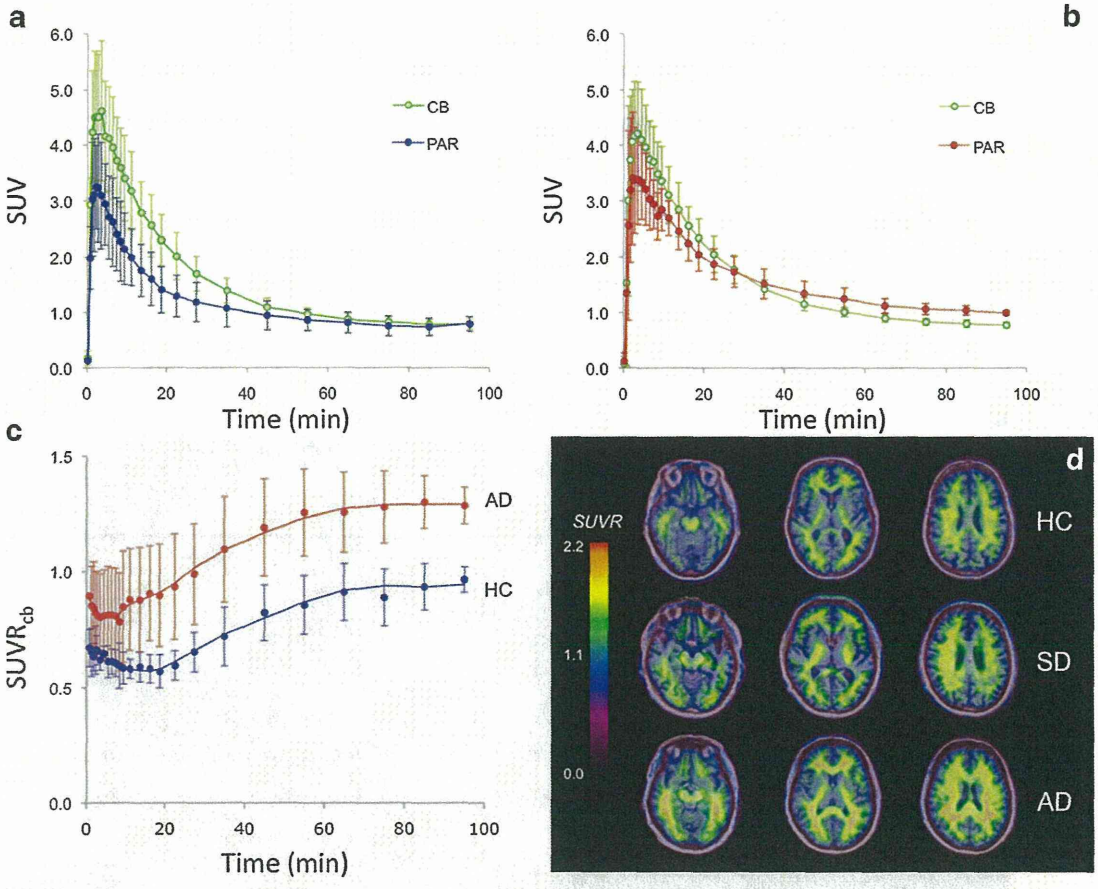

Fig. 1 ^{18}F-THK523 binding. Time-radioactivity curves for ^{18}F-THK523 in the parietal cortex (*PAR*) and the cerebellar grey matter (*CB*) in healthy controls (*HC*) (**a**) and Alzheimer's disease (*AD*) patients (**b**). There is fast ^{18}F-THK523 uptake in the brain followed by a fast clearance phase. While there is slower clearance with significantly higher retention in the parietal cortex of AD patients compared to HC, there are no significant differences in the cerebellar cortex uptake and clearance, further validating its use as reference region. **c** The total to non-specific binding ratios curves show significantly higher ^{18}F-THK523 retention in the parietal cortex of AD patients compared to HC. The specific binding reaches a plateau by 50 min post-injection. **d** Representative ^{18}F-THK523 PET images at three different brain levels in a 69-year-old female HC (MMSE 30, *top row*), a 73-year-old male semantic dementia (*SD*) patient (MMSE 21, *middle row*) and a 72-year-old female AD patient (MMSE 22, *bottom row*). Visual inspection of the images reveals no differences in ^{18}F-THK523 retention between HC and SD. There is higher white matter retention in AD compared to HC and SD. Data expressed as mean±SD of ten HC and ten AD patients

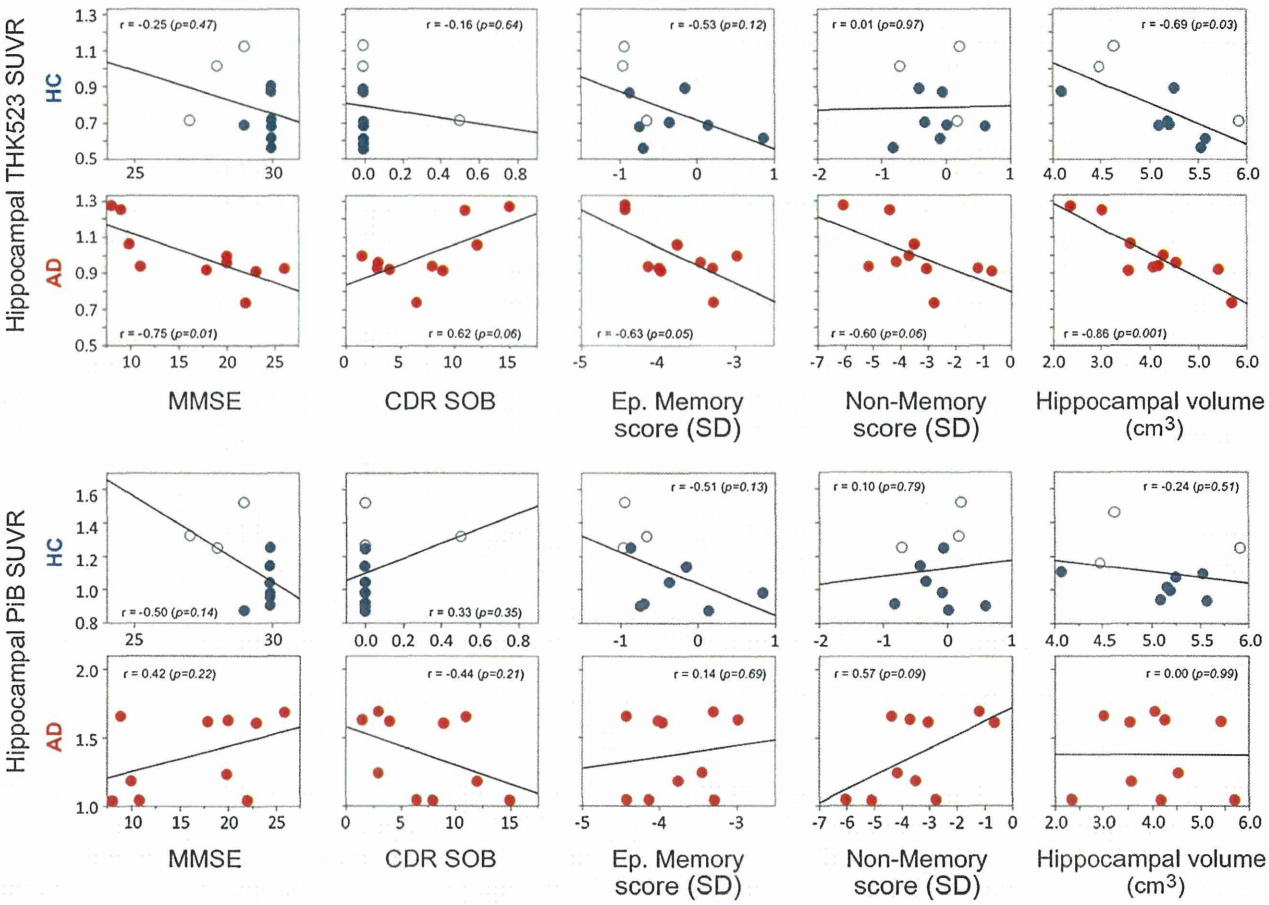

Fig. 3 Relationship between hippocampal ^{18}F-THK523 and ^{11}C-PIB retention with cognition and hippocampal volume. Regression analysis shows that while hippocampal ^{18}F-THK523 retention is not associated with cognition in HC, it is strongly associated with different cognitive parameters in AD patients (*top two rows*). On the other hand, hippocampal ^{18}F-THK523 retention is strongly associated with hippocampal volume in both HC and AD patients. There was no association between hippocampal ^{11}C-PIB retention (*bottom two rows*) with either cognitive parameters or hippocampal volume in any of the groups examined. All correlations were adjusted for age

hippocampus and insula was significantly higher than PIB–HC, but not significantly different from AD (Fig. 2).

Association between THK523 retention, cognition and brain volumetrics

While providing evidence of the general direction of the association between the different parameters (e.g. higher tau burden, lower cognitive performance), the associations derived from assessing all groups together tend to yield spurious correlations driven by the significant differences between the clinical groups. In order to avoid this issue, the associations with cognition and brain volumetrics were assessed in each clinical group separately.

In the case of THK523, there were no associations between cortical THK523 retention and cognitive parameters in HC, with the exception of the insula associated with episodic memory scores (r=−0.70, p=0.026). In the AD group, hippocampal THK523 retention was significantly associated with MMSE (r=−0.75, p=0.01) and episodic memory (r=−0.63, p=0.05) (Fig. 3). In the AD group, a strong trend was also observed between hippocampal THK523 retention, CDR SOB (r=0.62, p=0.055) and non-memory scores (r=−0.60, p=0.056). In regard to brain volumes, only hippocampal THK523 retention was significantly associated with hippocampal volume in both the HC (r=−0.69, p=0.03) and AD (r=−0.86, p=0.001) groups (Fig. 3). There were no correlations between global THK523 retention and cortical grey matter volume in any of the groups.

In the case of PIB, there were associations between PIB retention and MMSE in the orbitofrontal (r=−0.67, p=0.034), anterior (r=−0.65, p=0.04) and posterior cingulate (r=−0.78, p=0.007) regions of HC. In AD, there were some associations between PIB retention and cognitive parameters, but these correlations were, in every case, in the opposite direction as expected, where PIB retention in the anterior cingulate gyrus was positively associated with MMSE (r=0.63, p=0.049),